WAKEFIELD INDUCED ENERGY SPREAD IN THE FERMI UNDULATOR

A.A.G. Lutman*, M. Castronovo†, R. Vescovo*, Università degli Studi di Trieste, Trieste, Italy
C. Bonţoiu, P. Craievich‡, L. Rumiz, ELETTRA, Trieste, Italy

Abstract

The FERMI Project aims to achieve very high-brightness photon beam pulses of minimum bandwidth. These goals can be marred by the presence of large wakefields along the undulator small-gap vacuum chamber. Estimations of the induced energy-spread caused by the resistive wall and surface roughness wakefields along the FERMI FEL undulator are presented. The energy spread and losses induced by resistive wall wakefield are determined for three possible transverse geometries of the vacuum chamber, namely circular, rectangular and elliptic cross-section, while the energy spread and losses induced by the surface roughness wakefields are obtained for the circular cross-section case. In this last case in-house surface profile measurements carried on a spare vacuum chamber of ELETTRA are used to provide realistic estimates.

WAKEFIELDS IN THE UNDULATOR VACUUM CHAMBER

In the undulator vacuum chamber the finite conductivity of the metal wall and the roughness of the chamber inner surface wakefields are sources of wakefields. For the FEL effect, the main concern is the longitudinal wake which may impress an energy modulation on the electron bunch and consequently degrade the quality of the FEL radiation. Transverse wakefields are much less disruptive in the undulator and will be neglected.

Resistive Wall Wakefields

The interaction between the electron beam and the metal wall has been evaluated for circular, rectangular and elliptical cross-section vacuum chambers. Regardless of the shape of the cross-section, the chamber is modeled as an infinite pipe with finite conductivity σ, electron relaxation time $\tau > 0$ and infinite wall thickness. The relative longitudinal displacement from the bunch head will be denoted by z. The almost flat-top short bunches which will be used for the FERMI FEL contain very high frequencies components induced by the residual current spikes and thus require, as pointed out by Bane [1], the use of the AC conductivity model. In the following formulas the skin-depth related parameter $\lambda = \sqrt{\frac{Z_0 \sigma |k|}{2}}(i + sign(k))$ will be used, where Z_0 is the intrinsic impedance of the vacuum and k is the wave number.

Circular cross-section: For the circular cross-section, the calculations rely on the formula derived by Chao [2]. Denoting with b the radius of the pipe, the longitudinal coupling impedance is given in SI units by:

$$Z(k) = \frac{Z_0}{4\pi} \frac{1}{b} \frac{2}{\frac{\lambda}{k} - \frac{ikb}{2}} \tag{1}$$

Rectangular cross-section: For the rectangular shape the evaluation relies on the formulas given by Henke and Napoly [3]. Although the theory is elaborated for two conducting infinite parallel plates, we will use it for a rectangular cross-section neglecting the effects of the lateral walls. Denoting with b the half gap between the metal plates, the longitudinal coupling impedance, as given in [4] is in SI units:

$$Z(k) = \frac{Z_0}{4\pi} \int_{-\infty}^{+\infty} \frac{1}{\frac{\lambda}{k} \cosh^2 bx - \frac{ik}{x} \cosh bx \sinh bx} dx \tag{2}$$

Elliptic cross-section: For the elliptic cross-section shape a novel method that holds for AC conductivity and allows one to evaluate the wakes at very short range, has been developed. The fields are obtained by developing a system of solutions to the Maxwell's equations both in the vacuum and in the resistive wall and then imposing the boundary conditions on the wall surface similar to what has been done for the circular case. The longitudinal and transverse wake functions are then calculated using field expansions. Maxwell's equations have been solved in an elliptic cylindrical system of coordinates (u, v, z) (see Fig. 1), taking the source as an ultrarelativistic point charge travelling down the pipe, parallel to its axis, located arbitrarily in (u_1,v_1,0). On the cross-section the interface between the vacuum and the metal wall is the ellipse of equation $u = u_0$. With the observation that, due to causality, any field must vanish for $z > 0$, the Fourier transform of the electric and magnetic longitudinal fields in the vacuum, can be written as:

$$\begin{aligned} \tilde{E}_z &= \sum_{n=0}^{+\infty} A_n \cosh nu \cos nv + \sum_{n=1}^{+\infty} B_n \sinh nu \sin nv \\ c\tilde{B}_z &= \sum_{n=0}^{+\infty} B_n \cosh nu \cos nv - \sum_{n=1}^{+\infty} A_n \sinh nu \sin nv \end{aligned} \tag{3}$$

where A_n and B_n depend on k and are determined by imposing the continuity of the fields $\tilde{E}_z$, $\tilde{B}_z$, $\tilde{E}_v$, $\tilde{B}_v$. In the vacuum, the transverse fields behavior shows a coupling between different modes. In detail the components $\cos nv$,

* DEEI
† Dipartimento di Fisica
‡ paolo.craievich@elettra.trieste.it

$\sin nv$ depend on the $(n-2)$-th, n-th and $(n+2)$-th coefficients. Maxwell's equations in the metal wall, solved by separation of variables, lead to the angular and radial Mathieu functions [5]. For small skin-depth values, the series

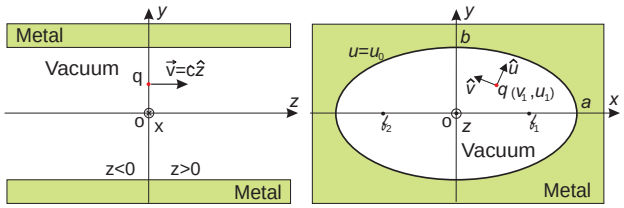

Figure 1: Elliptic cylindrical system of coordinates and the source point charge.

of products of Bessel and Hankel functions for the Mathieu radial functions can be approximated and the boundary conditions yield a tridiagonal infinite linear system for the coefficients A_n and B_n which can be truncated to calculate explicitly the coefficients. Since in the coefficients matrix there is no relation between A_n and B_n, neither between A_{2n} and A_{2n+1} nor between B_{2n} and B_{2n+1}, the whole system can be split up in four independent parts. To solve a truncated tridiagonal subsystem for the first $M+1$ coefficients, the following formula can be used:

$$\begin{cases} X_M = & \dfrac{T^c_M}{C_M} \\ X_n = & \dfrac{T^c_n - z_n X_{n+1}}{C_n} \quad n = 0..M-1 \end{cases} \tag{4}$$

where:

$$\begin{aligned} C_n &= \begin{cases} d_0 & n=0 \\ d_n - \dfrac{s_{n-1}z_{n-1}}{C_{n-1}} & n=1..M \end{cases} \\ D_n &= \dfrac{s_{n-1}}{C_{n-1}} \qquad n=1..M \\ T^c_n &= \begin{cases} t_0 & n=0 \\ t_n - T^c_{n-1}D_n & n=1..M \end{cases} \end{aligned}$$

s_n, d_n, z_n and t_n are yet to be defined for each kind of coefficient, but in the case of the longitudinal wake-function, if the leading charge is on axis, only the A even subsystem is excited and all other coefficients are zero. Denoting with a and b respectively the major and the minor half axis of the cross-section, with $l = \sqrt{a^2 - b^2}$ the half focal length and $h = l\sqrt{\cosh^2 u - \cos^2 v}$ the metric, the following formula for the A even subsystem has been obtained:

$$\begin{aligned} d_n &= -\frac{ikl^2}{\cosh 2nu_0}\left[\frac{\sinh(4n+2)u_0}{8(2n+1)} + \frac{\sinh(4n-2)u_0}{8(2n-1)}\right] + \\ &\quad + \left[\frac{i}{k} + \frac{2ik}{\lambda^2}\right] 2n \sinh 2nu_0 + \\ &\quad + l\cosh u_0 \left[\frac{k}{\lambda}\frac{\cosh 4nu_0}{\cosh 2nu_0} + \frac{\lambda \cosh 2nu_0}{k}\right] \\ s_n &= \frac{ikl^2(1+\delta_{n0})}{8(2n+1)}\frac{\sinh(4n+2)u_0}{\cosh 2(n+1)u_0} \\ z_n &= \frac{ikl^2}{8(2n+1)}\frac{\sinh(4n+2)u_0}{\cosh 2nu_0} \\ t_n &= -\frac{q}{(1+\delta_{n0})\pi\epsilon_0}\frac{\cos 2nv_1 \cosh 2nu_1}{\cosh 2nu_0} \\ n &= 0..M \end{aligned} \tag{5}$$

The Lorentz force due to the leading charge experienced, by a trailing charge q_t travelling down the pipe at the speed of light with coordinates (u, v, z) is:

$$\begin{cases} F_L = q_t E_z \\ \boldsymbol{F}_T = q_t\left[\hat{u}\left(E_u - B_v\right) + \hat{v}\left(E_v + B_u\right)\right] \end{cases} \tag{6}$$

where L denotes longitudinal and T transverse. The longitudinal wake function is obtained by numerically inverse Fourier transforming $\tilde{E}_z$ in (3), while using the relations:

$$\begin{cases} \tilde{E}_v + c\tilde{B}_u = -\frac{i}{hk}\frac{\partial \tilde{E}_z}{\partial v} \\ \tilde{E}_u - c\tilde{B}_v = +\frac{i}{hk}\frac{\partial c\tilde{B}_z}{\partial v} \end{cases} \tag{7}$$

The transverse force is obtained numerically inverting the term:

$$\frac{i}{hk}\left(\hat{u}\frac{c\partial \tilde{B}_z}{\partial v} - \hat{v}\frac{\partial \tilde{E}_z}{\partial v}\right) \tag{8}$$

Next the elliptic cross-section resistive wake function is plotted for several values of the ratio a/b, including the limiting cases $a/b = 1$ and ∞, using the materials specified in Table 1.

Table 1: Conductivity and relaxation time for Al and Cu.

	Aluminium	Copper
$\sigma\ [\Omega^{-1}m^{-1}]$	$4,22 \times 10^7$	$6,45 \times 10^7$
$\tau\ [s]$	$8,00 \times 10^{-15}$	$2,70 \times 10^{-14}$

As shown in Figs. 2 and 3 the peaks of the longitudinal wake functions continuously decrease from the circular case to the parallel plates. The wake functions obtained using copper as material for the vacuum chamber present more oscillations which are due to the higher electron relaxation time.

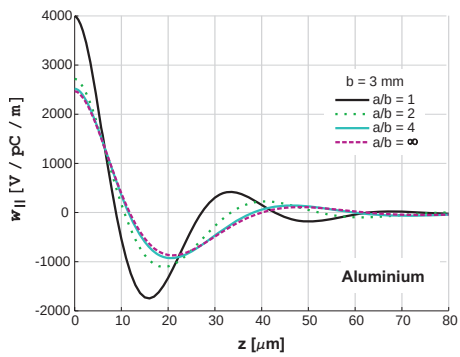

Figure 2: Longitudinal resistive wall wake functions for aluminium made walls and $b = 3$ mm.

Surface Roughness Wakefields

The interaction between the beam and the surface roughness of the undulator vacuum chamber is yet another source of energy spread which could impact FEL process. To a

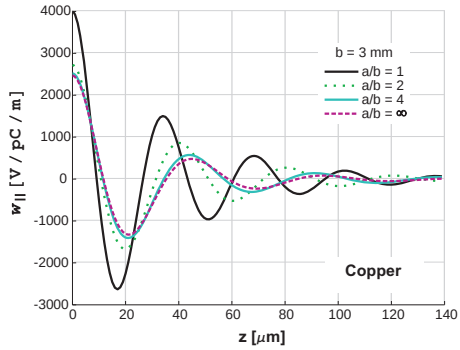

Figure 3: Longitudinal resistive wall wake functions for copper made walls and $b = 3$ mm.

first approximation the surface roughness makes the vacuum chamber behave like a disk-loaded cavity; there will be a continuous change of energy between the beam and what is called a synchronous field mode [6, 7]. Furthermore, if the roughness can be approximated by a collection of bumps whose tangent to the smooth wall is small, there will be one more contribution to the total roughness wakefield coming from their individual impedance, averaged over a certain distribution function [8].

Surface analysis: Several AFM surface scans (see Fig.4) have been carried on a spare vacuum chamber of the ELETTRA storage ring [9] in order to obtain information on the average peak height and periodicity of the roughness.

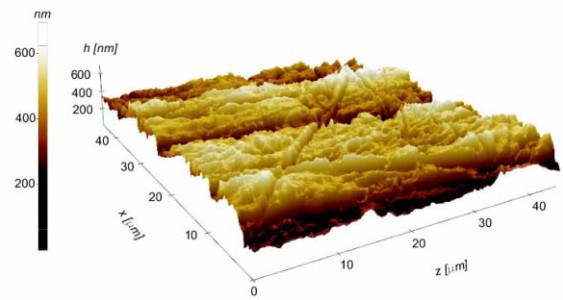

Figure 4: Measured 3D surface profile.

First, it is necessary to distinguish between the long and short range variation of the surface-vacuum boundary. Thus, a longitudinal scan over 120 μm has been filtered (Gaussian filter of 15 μm standard deviation) separating out a low-frequency surface component from a high-frequency component, (see Fig. 5). Fourier transforms of these two components reveal their frequency content $\nu = \frac{c}{\lambda}$ which together with the rms height h_{rms} makes it possible to fit them to a sinusoidal corrugation model. It turns out that the low frequency content can be treated within the resonator model with some corrections due to the very small size of the roughness height [7], while the high frequency component, due to its higher aspect ratio, can be considered within

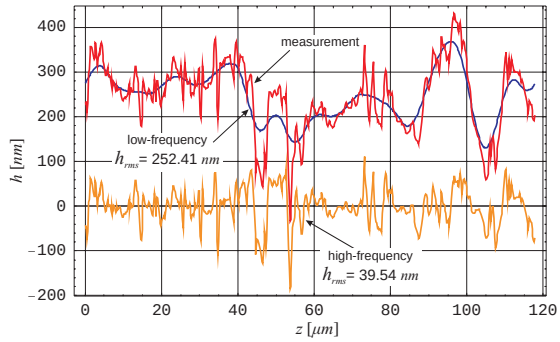

Figure 5: A Gaussian filter is applied to the real surface profile (red) in order to detach its low (blue) and high (orange) frequency components

Table 2: Overview of the corrugation parameters.

Component	λ	h_{rms}	$AR = \lambda/h_{rms}$
low-frequency	30 μm	250 nm	120
high-frequency	10 μm	40 nm	250

the Stupakov's statistical (small-angle) model [8].

Surface wakefield in circular cross-section pipes: Within the modified resonator model proposed by Stupakov [7], the roughness wake function has a cos-like variation of constant amplitude and is defined as:

$$w_{||}(z) = \frac{Z_0 c}{4\pi} \frac{h_{rms}^4 \kappa^6}{64} \cos k_0 z \qquad (9)$$

where $\kappa = 2\pi/\lambda$, b is the vacuum chamber radius and $k_0 = \kappa/2$ is the rough synchronous mode, while the statistical model predicts a damped wake function with a singularity at $z = 0$:

$$w_{||}(z) = \frac{Z_0 c}{4\pi} \frac{h_{rms}^2 \kappa^2}{b} \frac{1}{2\sqrt{\pi}} \frac{\partial}{\partial z} \frac{\cos \frac{1}{2}\kappa z + \sin \frac{1}{2}\kappa z}{\sqrt{\kappa z}} \qquad (10)$$

Using the parameters in Table 2, both wake functions are plotted comparatively for b = 3 mm in Fig. 6.

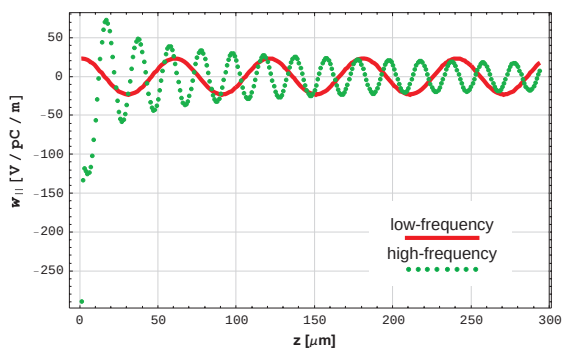

Figure 6: Surface roughness wake functions.

WAKEFIELD INDUCED ENERGY SPREAD

In this section some results concerning the induced energy spread for the medium bunch configuration of FERMI FEL [10] are presented considering contributions from the resistive wall and surface roughness wakefields.

Contribution of the electrical resistivity

Considering only Al for the vacuum chamber walls and AC conductivity, Fig. 7 shows the induced energy spread obtained through convolution between the circular/elliptic ($a/b = 6$)/rectangular (parallel plates) cross-section resistive wake functions and the longitudinal bunch profile mentioned above. Therefore, the rectangular cross-section with rounded lateral sides proposed in the FERMI CDR [10] can be replaced by an elliptic cross-section with $a/b > 6$ without changing the energy spread.

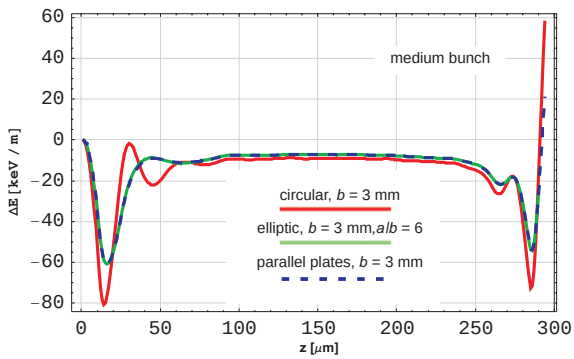

Figure 7: Resistive wall induced energy spread.

Surface roughness contribution

Convoluting separately the wake functions given by (9) and (10) with the medium bunch profile [10] the energy spread is obtained as shown in Fig. 8. As it can be seen, at

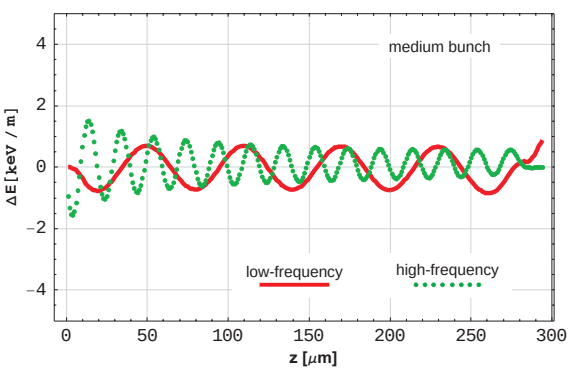

Figure 8: Roughness induced energy spread.

the core of the bunch the contribution of the low-frequency roughness component predominates over the contribution of the high-frequency roughness component both falling in the same range of magnitude.

CONCLUSIONS

Table 3 lists the maximum values of the energy spread in the useful part of the bunch (200 μm for the medium bunch and 350 μm for the long bunch). If the FERMI undulator would have vacuum chamber surface comparable with the one analyzed above, that is for AR = 120. In conclusion, it is recommended for the undulator vacuum chamber to be made of Aluminium, have a rectangular or elliptic cross-section. In what concerns the rectangular cross-section roughness wakefield, calculations are on the way and preliminary results show that the induced energy spread is 35-40 % lower than for the circular cross-section case. As for the surface, when $AR = 120$, the roughness induced energy spread accounts for about 17 % and 12 % of the resistive induced energy spread, respectively for the medium and long bunch.

Table 3: Estimated energy spread for the FERMI FEL undulator.

Source	short bunch	long bunch
Resistive wall	11.71 keV/m	9. 35 keV/m
Surface roughness	1.73 keV/m	1.17 keV/m
Total	13.44 keV/m	10.52 keV/m

REFERENCES

[1] K.L.F. Bane and G. Stupakov, "The Short Range Resistive Wall Wakefields", SLAC/AP-87, June 1991.

[2] A.W. Chao, "Physics of Collective Beam Instabilities in High Energy Accelerators", John Wiley & Sons, Inc. 1993.

[3] H.Henke and O.Napoly, "Wake Fields between two Parallel Plates", CERN/LEP-RF/89-71 CLIC Note 103, 1989.

[4] K.L.F Bane and G. Stupakov, "Resistive Wall Wakefield in the LCLS Undulator Beam Pipe", SLAC-PUB-10707.

[5] P.M.Morse and H.Feshbach, "Methods of Theoretical Physics", McGraw-Hill, New York, 1953.

[6] A. Novokhatski and A. Mosnier, "Wakefields of short bunches in canal covered with thin dielectric layer", PAC 1997, p.1661.

[7] G.V. Stupakov, "Surface roughness impedance", SLAC-PUB-8743, December, 2000.

[8] G.V. Stupakov, "Impedance of small obstacles and rough surface", Phys. Rev. ST-AB, Vol.1, 064401 (1998).

[9] A. Gambitta et al., Experience with aluminium vacuum chambers at Elettra, Proceedings of EPAC 2000, Vienna, Austria;

[10] FERMI@Elettra Conceptual Design Report, to be published.